Superconductor Science and Technology

PAPER

Hybrid Nb/Al/$Ba_{0.5}K_{0.5}Fe_2As_2$ sandwich Josephson junctions

To cite this article: Wanghao Tian *et al* 2020 *Supercond. Sci. Technol.* **33** 025014

IOP Publishing Superconductor Science and Technology
Supercond. Sci. Technol. 33 (2020) 025014 (7pp) https://doi.org/10.1088/1361-6668/ab601f

Hybrid Nb/Al/$Ba_{0.5}K_{0.5}Fe_2As_2$ sandwich Josephson junctions

Wanghao Tian[1], Yangyang Lv[1], Zuyu Xu[1], Huili Zhang[1], Shixian Chen[1], Sining Dong[1], Jun Li[1], Yong-Lei Wang[1], Dieter Kölle[2], Reinhold Kleiner[2,3], Huabing Wang[1,3] and Peiheng Wu[1]

[1] Research Institute of Superconductor Electronics, Nanjing University, Nanjing 210023, People's Republic of China
[2] Physikalisches Institut and Center for Quantum Science in LISA$^+$, Universität Tübingen, D-72076 Tübingen, Germany

E-mail: kleiner@uni-tuebingen.de and hbwang@nju.edu.cn

Received 22 September 2019, revised 28 November 2019
Accepted for publication 9 December 2019
Published 8 January 2020

Abstract

We fabricated hybrid Josephson junctions between a $Ba_{0.5}K_{0.5}Fe_2As_2$ (BKFA) single crystal and the conventional superconductor Nb with normal metal Al as the barrier. An *in situ* process was used to create clean BKFA/Al/Nb interfaces. Current transport is along the *c*-axis of BKFA. The current–voltage characteristics are slightly hysteretic at low temperatures. Except for some features indicative of resonant modes the shape of the current–voltage characteristics can be well described by the resistively and capacitvely shunted junction (RCSJ) model, with a product of the Josephson critical current and the normal state resistance of the junction exceeding 180 μV at low temperatures. The temperature dependence of the Josephson current is linear for temperatures down to 2 K. Under 40 GHz microwave irradiation integer Shapiro steps are observed. The power dependence of the Shapiro step-height is in good agreement with RCSJ simulations. Possible relations of our data with the symmetry of the superconducting order parameter of BKFA are discussed.

Keywords: Josephson junctions, iron-based superconductors, pairing symmetry

(Some figures may appear in colour only in the online journal)

1. Introduction

The iron-based superconductors are a new class of high-temperature superconductors following the cuprates, attracting great interest both in terms of fundamental physics and in terms of applications [1–3]. Of particular interest for superconducting electronics and also for basic studies are Josephson junctions. The fabrication of such devices from iron-based superconductors and their detailed characterization is still in its infancy, motivating the present study. Apart from issues related to the quality of interfaces between different materials there is also the question to what extent a potential unconventional order parameter affects the junction properties. Different pairing symmetries have been proposed, such as single-gap *s*- or *d*-wave, mixtures of the form $s + id$ or the multiband order parameters $s_{\pm}$, s_{++} [1, 4–8]. The latter two order parameters are the most discussed ones. Here, the order parameter has *s*-wave symmetry on the different Fermi sheets but, for the $s_{\pm}$ case, the signs of the order parameters are different on different sheets.

The order-parameter symmetries can be studied by various experimental techniques, including nuclear magnetic resonance [9, 10], angle-resolved photoemission spectroscopy [11], impurity doping experiments [12] or scanning tunneling microscopy [13]. An interesting method is to make use of the Josephson effect because of its phase-sensitivity [14–17], allowing, e.g., to probe the sign change of an order parameter with $d_{x^2-y^2}$ symmetry. Relevant in our context are *c*-axis hybrid junctions between a cuprate and a conventional superconductor. In this geometry contributions of the *d*-wave order parameter to the Josephson current cancel, allowing to

[3] Authors to whom any correspondence should be addressed.

test the presence of *s*-wave components. Corresponding experiments have been performed on YBCO [18–22] and BSCCO [23], using Pb as the conventional superconductor.

Also for the case of iron-based superconductors one can expect that for order parameters that exhibit sign changes the contributions to the *c*-axis supercurrents will cancel at least partially. For the case of the multiband order parameters $s_{\pm}$ and s_{++} additional effects can occur. For example, depending on parameters, the temperature dependence of the Josephson critical current can differ strongly from conventional junctions [24–26]. In addition, under microwave irradiation an unusual dependence on the Shapiro-step heights as a function of microwave power and the appearence of fractional steps has been predicted [27].

For Fe-based superconductors there are relatively few reports on Josephson junctions; for reviews, see [8, 28]. Hybrid junctions with Pb, PbIn or Nb as counter electrodes were patterned on $NdFeAsO_{0.88}F_{0.12}$ polycrystals [29], $BaFe_{1.8}Co_{0.2}As_2$ thin films [30–33] or single crystals [34, 35], $Ba_{1-x}K_xFe_2As_2$ (BKFA) [25, 36] or $Ba_{1-x}Na_xFe_2As_2$ [37, 38]. All-pnictide junctions were fabricated from $BaFe_2As_2$ [39] or $BaFe_{1.84}Co_{0.16}As_2$ [31, 33] thin films and by interfacing $SrFe_{1.74}Co_{0.26}As_2$ and $Ba_{0.23}K_{0.77}Fe_2As_2$ single crystals [40]. Many of the hybrid junctions were designed as point contacts, not allowing, e.g., for well-defined temperature-dependent measurements. For planar hybrid junctions between BKFA and a conventional superconductor the only report known to us is [36], where non-optimally doped BKFA crystals with critical temperatures of 26 and 29 K were studied.

In the present work, we report on two planar hybrid *c*-axis $Nb/Al/Ba_{0.5}K_{0.5}Fe_2As_2$ Josephson junctions, where an *in situ* fabrication technique was used to minimize interfacial oxidation or degradation. Transport experiments were carried out for temperatures down to 2 K, in magnetic fields of up to 100 G and in microwave fields of up to 40 GHz. For sample A (sample B) The critical temperature of the BKFA crystal was $T_c = 39.2$ K (38.2 K), which is near optimal doping [41]. The onset of the superconducting transition of the Nb electrode is 8.7 K for sample A and 7.3 K for sample B. Zero resistance is reached at 6.8 K for sample A and at 6.5 K for sample B. For the Josephson critical current density near 3 K we find a value around 150 A cm^{-2} for sample A and 100 A cm^{-2} for sample B. Such values are at not unusual for Josephson junctions. The product I_cR of the Josephson critical current and the normal state resistance of sample A is 158 μV at 3.1 K while for Sample B we find a somewhat lower value of 134 μV at 3.0 K. These values for the I_cR products are very high for Josephson junctions involving iron-based superconductors, although an order of magnitude lower than the I_cR values of, say, high-quality Nb tunnel junctions. Most of the properties we see are not unusual for Josephson junctions, with the exception of a strikingly linear temperature dependence of the critical current down to the lowest bath temperatures. This is in-line with other reports on iron-based Josephson junctions but rarely, if at all, seen for other junctions.

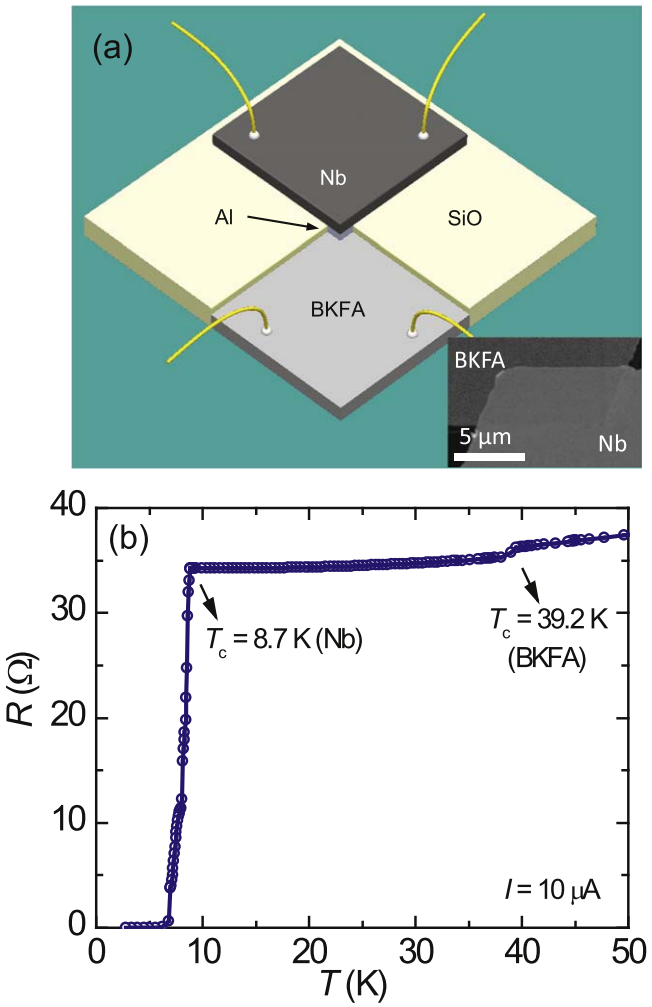

Figure 1. (a) Sketch of the junction geometry. The inset shows a scanning electron microscopy image of the overlap region between BKFA and Nb. (b) Temperature dependence of the junction resistance of sample A measured in a four-probe configuration.

2. Sample fabrication

We discuss data for two junctions, sample A and sample B. Both junctions have the same geometry, which is sketched in figure 1(a). A 10 × 10 μm^2 quadratic junction is formed in the overlap region between Nb and BKFA. The inset in figure 1(a) displays a SEM image of the overlap region. In our fabrication process, cleaved BKFA crystals with a thickness of 200 nm (sample A) and 150 nm (sample B) are glued to sapphire substrates with epoxy. After 5 s of Ar ion etching to clean the surface of the crystal, an 8 nm thick Al layer is evaporated *in situ* on the crystals by electron beam evaporation, and then a 200 nm thick Nb layer is deposited using *in situ* magnetron sputtering deposition. Next, a right-angle corner is patterned into the BKFA/Al/Nb sandwich via ion beam milling and a 250 nm thick layer of SiO is evaporated preventing electrical shorts between the bottom electrode (BKFA) and the to-be-deposited Nb top electrode. During this process the BKFA/Al/Nb sandwich is covered by photoresist to allow a lift-off of the SiO layer in the junction area. After

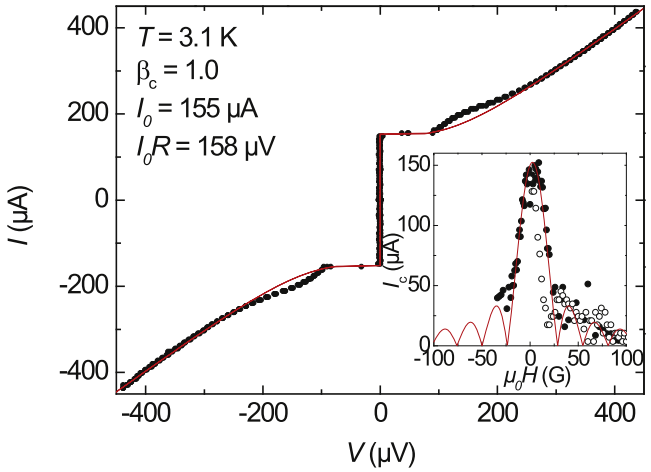

Figure 2. (a) IVC of sample A, as measured at a bath temperature of 3.1 K (solid circles). The line is a fit using the RCSJ model with a Stewart-McCumber parameter $\beta_c = 1$. I_0 is the noise-free critical current used in the simulations. The inset shows the magnetic field dependence of the critical current for sample A (solid circles) and sample B (open circles), for fields applied parallel to the in-plane junction edges. The line is the Fraunhofer pattern expected for a junction with homogeneous critical current density. The pattern has been shifted by 2.5 G to account for residual fields in the measurement setup.

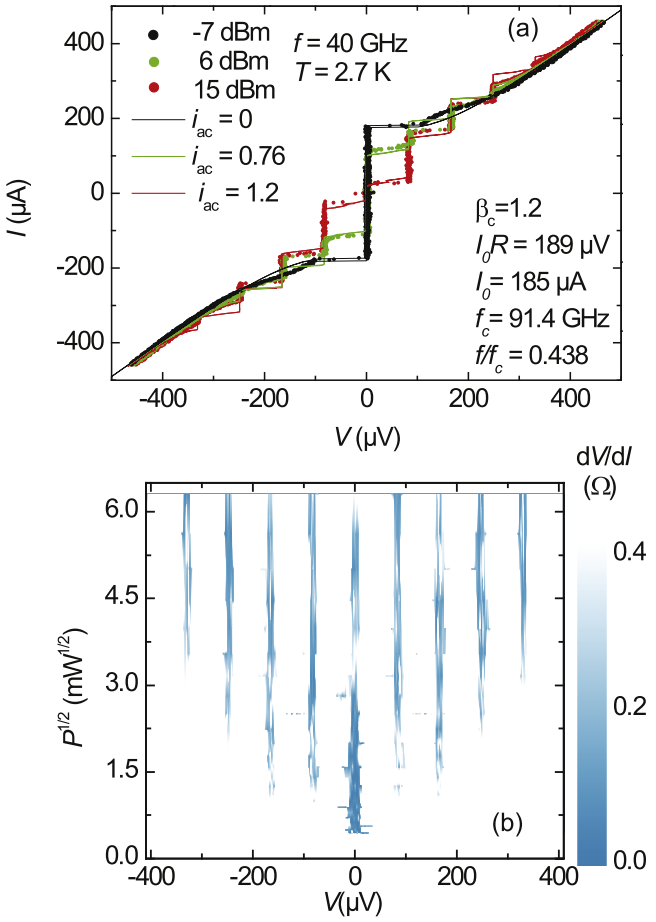

Figure 3. (a) IVCs of sample A in 40 GHz microwave fields at three different power levels, indicated in dBm, at a bath temperature of 2.7 K. Lines are fits using the RCSJ model. The ac current, normalized to I_0, is indicated. (b) Color plot of the differential resistance dV/dI in the IVCs under 40 GHz microwave irradiation as a function of microwave amplitude $P^{1/2}$ and voltage V across the stack.

lift-off a second Nb is deposited, with a thickness of 200 nm. The structure is finally etched down using reactive ion etching to form the junction and the contacting electrodes.

Figure 1(a) shows the resistance versus temperature curve of sample A for temperatures between 50 and 2 K. For decreasing temperature there is a first drop in resistance at 39.2 K which is the critical temperature of the BKFA crystal. The resistance strongly decreases below 8.7 K and reaches zero at 6.8 K. As we will see below the actual junction resistance is about 1 Ω, thus the resistive transition below 8.7 K and particularly the foot structure between 8 and 6.8 K reflects the resistive transitions of the two Nb layers. The Nb layer interfacing the Al is presumably the one having a slightly reduced T_c-onset of about 8 K.

3. Results

Figure 2 shows by solid circles the IVC of sample A, as measured at a bath temperature of 3.1 K. At the critical current $I_c = 152\ \mu$A the voltage jumps to a value of about 98 μV and then increases continuously with increasing current. Near I_c there is in fact a tiny hysteresis which increases when going to lower temperatures, see figure 3. The solid line in figure 2 is a numerical simulation based on the resistively and capacitively shunted junction (RCSJ) model [42, 43], where we used a Stewart–McCumber parameter $\beta_c = 2\pi I_0 R^2 C/\Phi_0 = 1$. Here, I_0 is the Josephson critical current in the absence of thermal fluctuations, R is the junction resistance, C is the junction capacitance and Φ_0 is the flux quantum. Note that the good agreement between the measured and the simulated IVCs at large currents imply that there is no or at least no significant excess current. In the simulations we included also thermal noise, leading to a critical current I_c, which is slightly lower than I_0. Comparing simulations and measurement one finds $I_0 = 155\ \mu$A, $R = 1.02\ \Omega$ and $I_0R = 158\ \mu$V. This value is actually about a factor of 20 larger than I_0R reported for the planar junction in [36] for the same bath temperature, and e.g. about by a factor of 50 larger than the I_0R values reported in [38]. The I_0R product we observe is however in the range of values obtained with point contacts [36], although below the value reported in [35] for a SIS-type junction. We further find for the product of resistance and junction area a value around $RA = 10^{-6}\ \Omega\,\mathrm{cm}^2$ which is three orders of magnitude lower than typical RA products of tunnel junctions. The RA value we observe is relatively high for good SNS junctions but comparable to the corresponding values obtained e.g. in [36]. From $\beta_c = 1$ we further find a junction capacitance of about 2 pF, which might arise from stray fields between the Nb electrode and the substrate. We further note that the observed β_c value around 1 seems to be much higher and consequently the damping of our junction much lower than that of most other

hybrid Fe-based junctions we are aware of, with the exception of the junctions reported in [33, 35]. The reduced damping may help in detecting dynamic effects such as internal resonances. The Stewart-McCumber parameter can also be written as $\beta_c = (f_c/f_{pl})^2$ where $f_c = I_0R/\Phi_0$ is the characteristic frequency and f_{pl} is the Josephson plasma frequency. We find a value of about 76 GHz for both frequencies.

Comparing the experimental and the simulated curves in figure 2 one observes a bump in the experimental IVC. The difference between the experimental and the theoretical curve is largest for a voltage near 150 μV, corresponding to a Josephson frequency of about 72 GHz. To explain the bump a first option is that it arises from a cavity resonance, i.e. a standing wave in the junction barrier. The frequency of the lowest cavity mode (one half wave along one side, no half-wave along the other) is $f_{cav} = c_s/2W$ with the junction length W and the Swihart velocity $c_s = 2\pi f_{pl}\lambda_J$. λ_J is the Josephson length. Using the expressions in [44] and the parameters of our junction we estimate c_s to be about 10^7 m s^{-1} and λ_J to be about 20 μm. This results in a cavity resonance frequency of 500 GHz which seems to be too high to explain the bump. Further, when increasing the magnetic field from zero the bump decreases in amplitude and disappears for field around 20 G. With increasing field its maximum slightly shifts, from about 150 μV and $\mu_0H = 0$ to roughly 100 μV for $\mu_0H =$ 20 G. By contrast, for a cavity resonance one would have expected that the hump increases with increasing field, reaching its maximum for a field near the first zero of the Fraunhofer pattern. As we will see below the voltage position of the bump decreases with increasing temperature and it further gets suppressed in microwave fields. The temperature shift of the bump voltage, as well as its shift in magnetic fields speaks against parasitic resonances somewhere on the substrate as its origin, because those resonances should be in essence temperature independent. An option which we cannot fully rule out is that the bump is caused by some Andreev-type processes. However, these processes typically lead to a finite excess current in the IVCs which seems to be absent in the IVCs of our samples. An intriguing speculation would be to consider the bump to arise from an out-of-phase Josephson plasma mode which can occur within a s-wave/$s_\pm$ wave hybrid junction [45]. Depending on parameters the frequency of this mode can be smaller or larger than the standard Josephson plasma frequency and can even become zero (Leggett mode). However, we have not enough information to substantiate this speculation. We finally note that a similar bump seems to be present in the IVCs presented in [35] for a SIS-type PbIn/TiO_2/$BaFe_{1.94}Co_{0.06}As_2$ hybrid junction.

The inset of figure 2 shows the magnetic field dependence of the critical current for two junctions (sample A, solid circles and sample B, open symbols). In fact, both samples got destroyed before completing the measurements for negative fields. If the Josephson critical current density were homogeneous one would expect a Fraunhofer pattern for I_c versus H, as indicated by the solid line in the figure. As one can see the experimental curve show some modulations, but the side maxima are not developed very well. This indicates

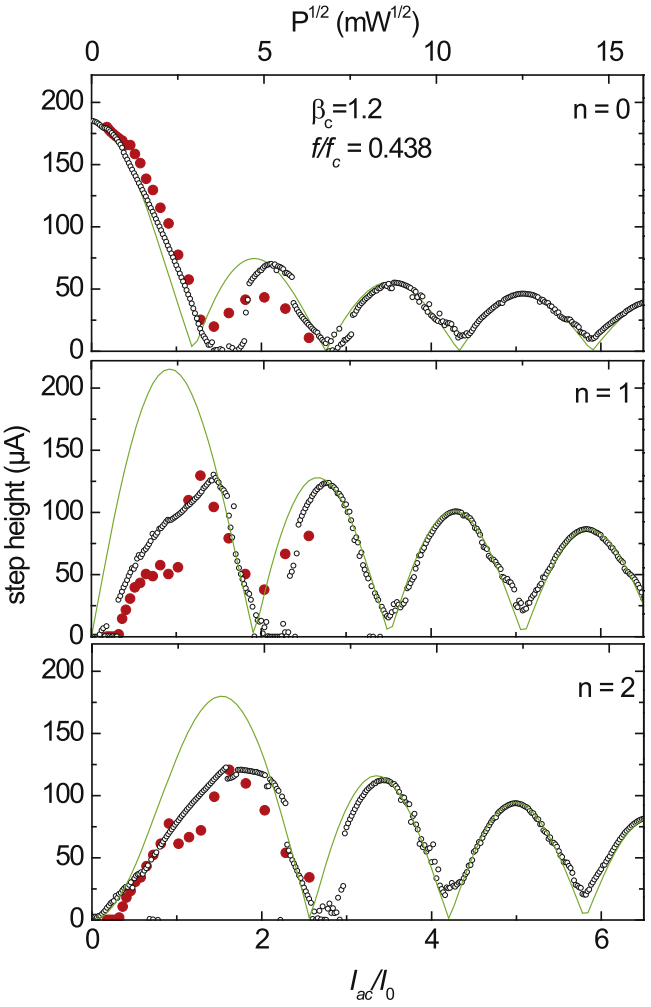

Figure 4. Critical current (upper graph) and the heights of the first and second Shapiro step (middle and lower graph) as a function of microwave amplitude at a microwave frequency of 40 GHz. Experimental data are displayed by solid (red) circles. The microwave amplitude is shown on the top axis. Open circles correspond to results from RCSJ simulation, the ac current, normalized to I_0 is shown on the bottom axis. The lines correspond to Bessel functions $J_n(x)$ with $n = 0$ (top graph), $n = 1$ (middle graph) and $n = 2$ (lower graph), with $x = V_{ac}/\Phi_0 f$, where V_{ac} is the applied ac voltage across the junction. x is chosen to match the RCSJ dependencies at large ac power. Parameters not displayed in the graph are the same as in figure 3.

that the homogeneity of the junctions is reasonable but not perfect. The zeroes of the Fraunhofer pattern are determined by the width of the junction and its effective thickness, which depends on the London penetration depth and the electrode thickness [44]. For our junctions we expect the zeroes to occur at multiples of 15 $\pm$ 2 G. In experiment we see that the first I_c minimum is at somewhat higher fields (26 G for sample A and 18 G for sample B). This may indicate that the actual width of our junctions is smaller than the nominal value.

Figures 3 and 4 show microwave response for sample A, measured at a frequency $f = 40$ GHz and a bath temperature of 2.7 K. In figure 3(a) we display three IVCs, taken at

microwave powers of, respectively, −7 dBm (0.2 mW), 6 dBm (4 mW) and 15 dBm (31.6 mW). While the IVC at 0.2 mW is in essence indistinguishable from the curve without microwaves (not shown), we see that for 4 mW three Shapiro steps have developed at voltages $V = n\phi_0 f$, with n up to 3. At 31.6 mW one observes Shapiro steps with n up to 4. No subharmonic steps appeared in either the 40 GHz measurements nor at measurements taken at lower frequencies. For 40 GHz this is displayed in more detail in figure 3(b), where we plot as a color scale the differential resistance of the IVCs for values below 0.4 Ω as a function of microwave amplitude $P^{1/2}$ and voltage V across the junction. The Shapiro steps appear as the dark colored vertical lines at integer n. To compare our data with theory we performed simulations witin the RCSJ model, using $\beta_c = 1.2$ and $I_0R = 185\,\mu$V, corresponding to $f_c = 91.4$ GHz. In the RCSJ model the microwave fields enter as an ac current, the amplitude of which is indicated in figure 3 normalized to I_0. The experimental IVCs and the simulated ones match reasonably well for all microwave amplitudes. In figure 4 we display by solid (red) symbols the critical current ($n = 0$) and the height of the first and second Shapiro step at a function of the microwave amplitude delivered from the microwave source (top axis). The open circles in the graphs correspond to RCSJ simulations, with the normalized ac current indicated on the bottom axis. We used the same proportionality factor between I_{ac}/I_0 as in figure 3, thus there is no additional free parameter for the simulations shown in figure 4. As one can see, the experimental and simulated curves match reasonably, although not perfect. Note that in the region I_{ac}/I_0 between 1 and 2 both the simulated and the experimental step heights exhibit some jumps. Indeed, in the simulations this is a chaotic regime, and also in experiment we observe some instabilities in the IVCs in this region. Thus our conclusion is that the current-phase relation of our junction is close to sinusoidal, with peculiarities in the Shapiro step heights arising from chaotic phenomena. A similar conclusion has been drawn in [25] for a point junction oriented in c direction. For reference we also show by the solid lines the dependence of the step heights on microwave amplitude, that would have been obtained for an ac and dc voltage bias. In this case the height of the nth step is given by the nth Bessel function $J_n(x)$, where $x = V_{ac}/\Phi_0 f$. The value of x is not explicitly shown in the plots; we have chosen x so that the step heights match the RCSJ simulations at high microwave amplitude. One notes that the step heights for the voltage bias are far off from the RCSJ plots at low ac amplitudes.

We finally discuss the temperature dependence of IVCs and of the junction critical current, as measured for sample B. The corresponding data are shown in figure 5. The main graph displays I_c versus T by solid symbols. I_c values are shown on the left axis. For comparison we also show by open symbols (right axis) some I_c values for sample A for which we do not have a systematic I_c versus T measurement. The inset shows IVCs at 7 different temperatures between 2.4 and 6 K. Starting with the inset one observes that the IVCs, measured with increasing bias current, exhibit a bump feature below 60 μV which shifts to lower voltages with increasing

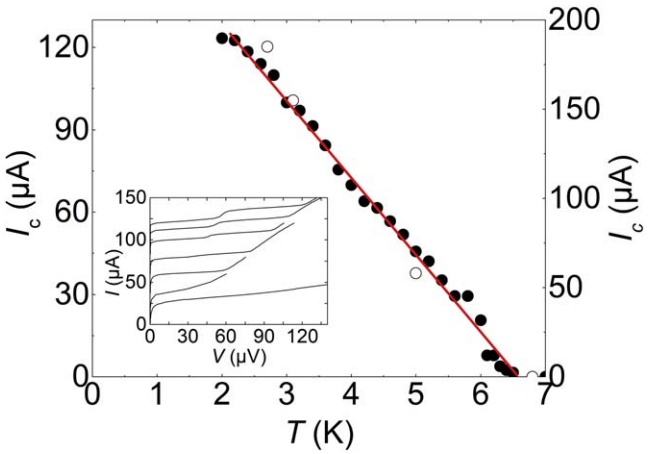

Figure 5. Temperature dependence of the critical current of sample B (solid symbols, left axis) and sample A (open symbols, right axis). The red line is a linear curve drawn to guide the eye. The inset shows IVCs of sample B at different temperatures: 2.4, 2.8, 3.2, 3.8, 4.6, 5.6 and 6 K from top to bottom.

temperature. Well above the critical current the junction resistance is about 1.17 Ω for temperatures below 5.6 K. Above 5.6 K the resistance strongly increases, presumably as a result of some parts of the Nb electrode getting resistive. Further note that the IVCs shown here are traced out only to voltages below 120 μV. The roughly linear part of the IVCs at high voltages could be part of another bump, like for junction A. We cannot decide this from our data. Returning to the main graph one notes that I_c versus T is linear for temperatures down to about 0.3 T_c, as indicated by the red straight line which is drawn as a guide to the eye. The linearity of I_c versus T down to about 0.3 T_c is striking but is also observed for other Fe-based Josephson junctions [28, 30–33, 36]. This seems to be the main feature that distinguishes this type of junctions from conventional SNS or SIS type junctions. In the SNS case, one expects a quadratic temperature dependence near T_c, while for SIS junctions I_c should start to saturate below about 0.6 T_c. Nearly linear I_c versus T curves are in the range of parameters of the formalisms presented in [26, 25]. The curves shown in [25] are for an (100) orientation but we assume that similar dependencies can be produced also for other directions of current flow. Indeed, this theory has been used in [38] to successfully fit I_c versus T curves of c-axis $Nb/Ba_{1-x}Na_xFe_2As_2$ junctions. In this case the I_c versus T curves were not completely linear but exhibited a weak negative curvature. The I_cR product observed for sample B is somewhat smaller than that of sample A, reaching a value of about 140 μV at 2 K. Ideally, I_cR could reach values of up to $(\Delta_{Nb} + \Delta_{max,BKFA})/e$, which would be as large as 9 mV at low temperatures [24]. Here, Δ_{Nb} is the niobium gap and $\Delta_{max,BKFA}$ is the maximum gap of BKFA. In the $s_\pm$ case the contributions to I_c having different signs of the order parameter in BKFA would cancel, leading to a strong reduction of I_cR. However, one should note that also conventional SNS-type Nb junctions [46], can have values of a few 10–100 μV, so that it is hard to draw clear conclusions from the I_cR product.

4. Summary

In summary we have fabricated planar *c*-axis Nb/Al/BKFA hybrid Josephson junctions, patterned on optimally doped BKFA single crystals. An *in situ* fabrication process was used to create clean interfaces between Nb, Al and BKFA. Transport experiments were carried out for temperatures down to 2 K, in magnetic fields of up to 100 G and in microwave fields of up to 40 GHz. Like for several other Fe-based Josephson junctions reported in the literature we find a remarkably linear temperature dependence of the Josephson critical current down to about $0.3\,T_c$. Our junctions are moderately underdamped at low temperature, allowing to observe resonant features in the current–voltage characteristic. It is tempting to associate the bump-like features we see to out-of-phase Josephson plasma modes predicted for an $s_{\pm}$ order parameter. However, also more conventional explanations are possible. Thus a clear conclusion on the BKFA order parameter cannot be given.

Acknowledgments

We gratefully acknowledge financial support by the National Natural Science Foundation of China (Nos. 61727805, 61521001, and 61771235), the National Key R&D Program of China (No. 2018YFA0209002), Jiangsu Key Laboratory of Advanced Techniques for Manipulating Electromagnetic Waves, the Priority Academic Program Development of Jiangsu Higher Education Institutions (PAPD), EU-FP6-COST Action CA16218, and the Deutsche Forschungsgemeinschaft via project KL93013/2.

ORCID iDs

Jun Li https://orcid.org/0000-0002-6928-1256
Huabing Wang https://orcid.org/0000-0003-4802-6077

References

[1] Hosono H and Kuroki K 2015 Iron-based superconductors: current status of materials and pairing mechanism *Physica* C **514** 399
[2] Si Q, Yu R and Abrahams E 2016 High-temperature superconductivity in iron pnictides and chalcogenides *Nat. Rev. Mater.* **1** 16017
[3] Hosono H, Yamamoto A, Hiramatsu H and Ma Y 2018 Recent advances in iron-based superconductors toward applications *Mater. Today* **21** 279
[4] Mazin I I 2010 Superconductivity gets an iron boost *Nature* **464** 183
[5] Reid J P *et al* 2012 From d-wave to s-wave pairing in the iron-pnictide superconductor (Ba, K)Fe_2As_2 *Supercond. Sci. Technol.* **25** 084013
[6] Böhm T, Kemper A F, Moritz B, Kretzschmar F, Muschler B, Eiter H-M, Hackl R, Devereaux T P, Scalapino D J and Wen H-H 2014 Balancing act: evidence for a strong subdominant d-wave pairing channel in $Ba_{0.6}K_{0.4}Fe_2As_2$ *Phys. Rev. X* **4** 041046
[7] Li J *et al* 2017 Nematic superconducting state in iron pnictide superconductors *Nat. Commun.* **8** 1880
[8] Yerin Y and Omelyanchouk A N 2017 Proximity and Josephson effects in microstructures based on multiband superconductors *Low Temp. Phys.* **43** 1013
[9] Grafe H J *et al* 2008 75As NMR studies of superconducting $LaFeAsO_{0.9}F_{0.1}$ *Phys. Rev. Lett.* **101** 047003
[10] Christianson A D *et al* 2008 Unconventional superconductivity in $Ba_{0.6}K_{0.4}Fe_2As_2$ from inelastic neutron scattering *Nature* **456** 930
[11] Richard P, Sato T, Nakayama K, Takahashi T and Ding H 2011 Fe-based superconductors: an angle-resolved photoemission spectroscopy perspective *Rep. Prog. Phys.* **74** 124512
[12] Li J, Guo Y F and Yang Z R 2016 Progress in nonmagnetic impurity doping studies on Fe-based superconductors *Supercond. Sci. Technol.* **29** 053001
[13] Yang H, Wang Z, Fang D, Deng Q, Wang Q H, Xiang Y Y, Yang Y and Wen H H 2013 In-gap quasiparticle excitations induced by non-magnetic Cu impurities in $Na(Fe_{0.96}Co_{0.03}Cu_{0.01})As$ revealed by scanning tunnelling spectroscopy *Nat. Commun.* **4** 2749
[14] Xu J H, Shen J L, Miller J H Jr and Ting C S 1994 Superconducting pairing symmetry and Josephson tunneling *Phys. Rev. Lett.* **73** 2492
[15] Harlingen D J Van 1995 Phase-sensitive tests of the symmetry of the pairing state in the high-temperature superconductors: Evidence for $d_{x^2-y^2}$ symmetry *Rev. Mod. Phys.* **67** 515
[16] Tsuei C C and Kirtley J R 2000 Pairing symmetry in cuprate superconductors *Rev. Mod. Phys.* **72** 969
[17] Klemm R A 2004 The phase-sensitive *c*-axis twist experiments on $Bi_2Sr_2CaCu_2O_{8+\delta}$ and their implications *Phil. Mag.* **85** 801
[18] Sun A G, Gajewski D A, Maple M B and Dynes R C 1994 Observation of Josephson pair tunneling between a high-T_c cuprate ($YBa_2Cu_3O_{7-\delta}$) and a conventional superconductor (Pb) *Phys. Rev. Lett.* **72** 2267
[19] Katz A S, Sun A G, Dynes R C and Char K 1995 Fabrication of all thin-film $YBa_2Cu_3O_{7-\delta}$/Pb Josephson tunnel junctions *Appl. Phys.Lett.* **66** 105
[20] Sun A G, Truscott A, Katz A S, Dynes R C, Veal B W and Gu C 1996 Direction of tunneling in Pb/I/$YBa_2Cu_3O_{7-x}$ tunnel junctions *Phys. Rev.* B **54** 6734
[21] Kleiner R *et al* 1996 Pair tunneling from *c*-axis $YBa_2Cu_3O_{7-x}$ to Pb: evidence for s-wave component from microwave induced steps *Phys. Rev. Lett.* **76** 2161
[22] Lesueur J, Aprili M, Goulon A, Horton T J and Dumoulin L 1997 Evidence for a Josephson tunnel current in all *in situ* c-$YBa_2Cu_3O_7$/Pb junctions *Phys. Rev.* B **55** R3398
[23] Mößle M and Kleiner R 1999 *c*-axis Josephson tunneling between $Bi_2Sr_2CaCu_2O_{8+x}$ and Pb *Phys. Rev.* B **59** 4486
[24] Ota Y, Nakai N, Nakamura H, Machida M, Inotani D, Ohashi Y, Koyama T and Matsumoto H 2010 Ambegaokar-Baratoff relations for Josephson critical current in heterojunctions with multigap superconductors *Phys. Rev.* B **81** 214511
[25] Burmistrova A V *et al* 2015 Josephson current in Fe-based superconducting junctions: theory and experiment *Phys. Rev.* B **91** 214501
[26] Nappi C, Romeo F, Sarnelli E and Citro R 2015 Quantum waveguide theory of the josephson effect in multiband superconductors *Phys. Rev.* B **92** 224503
[27] Ota Y, Machida M and Koyama T 2010 Shapiro steps as a direct probe of ±s-wave symmetry in multigap superconducting Josephson junctions *Phys. Rev.* B **82** 140509R

[28] Seidel P 2011 Josephson effects in iron based superconductors *Supercond. Sci. Technol.* **24** 043001
[29] Chen C-T, Tsuei C C, Ketchen M B, Ren Z-A and Zhao Z X 2010 Integer and half-integer flux-quantum transitions in a niobium-iron pnictide loop *Nat. Phys.* **6** 260
[30] Schmidt S, Döring S, Schmidl F, Grosse V, Seidel P, Iida K, Kurth F, Haindl S, Mönch I and Holzapfel B 2010 $BaFe_{1+8}Co_{0.2}$ As_2 thin film hybrid Josephson junctions *Appl. Phys. Lett.* **97** 172504
[31] Schmidt S, Döring S, Schmidl F, Tympel V, Haindl S, Iida K, Kurth F, Holzapfel B and Seidel P 2013 Bicrystalline grain boundary and hybrid SNS Junctions based on Ba-122 thin films *IEEE Trans. App. Supercond.* **23** 7300104
[32] Döring S *et al* 2015 Hybrid Josephson junctions with iron-based and conventional superconductor electrodes *J. Supercond. Nov. Magn.* **28** 1117
[33] Schmidt S, Döring S, Hasan N, Schmidl F, Tympel V, Kurth F, Iida K, Ikuta H, Wolf T and Seidel P 2017 Josephson effects at iron pnictide superconductors: Approaching phase-sensitive experiments *Phys. Status Solidi* B **254** 1600165
[34] Zhou Y-R, Li Y-R, Zuo J-W, Liu R-Y, Su S-K, Chen G F, Lu J L, Wang N L and Wang Y-P 2008 Phase-sensitive measurements on the corner junction of iron-based superconductor $BaFe_{1.8}Co_{0.2}As_2$ arXiv:0812.3295v1
[35] Hasan N, Reifert D, Döring S, Schmidt S, Tympel V, Schmidl F, Wolf T and Seidel P 2016 Planar hybrid Josephson junctions based on Ba-122 single crystals *IEEE Trans. Appl. Supercond.* **1051** 8223
[36] Zhang X H, Oh Y S, Liu Y, Yan L, Kim K H, Greene R L and Takeuchi I 2009 Observation of the Josephson effect in Pb/Ba_{1-x} $K_xFe_2As_2$ single crystal junctions *Phys. Rev. Lett* **102** 147002
[37] Fisun V V, Balkashin O P, Kvitnitskaya O E, Korovkin I A, Gamayunova N V, Aswartham S, Wurmehl S and Naidyuk Y G 2014 Josephson effect and Andreev reflection in Ba_{1-x} $Na_xFe_2As_2$ ($x = 0.25$ and 0.35) point contacts *Low Temp. Phys.* **40** 919
[38] Kalenyuk A A, Pagliero A, Borodianskyi E A, Kordyuk A A and Krasnov V M 2018 Phase-sensitive evidence for the sign-reversal $s_{\pm}$ symmetry of the order parameter in an iron-pnictide superconductor using Nb/Ba_{1-x} $Na_xFe_2As_2$ Josephson junctions *Phys. Rev. Lett.* **120** 067001
[39] Katase T, Ishimaru Y, Tsukamoto A, Hiramatsu H, Kamiya T, Tanabe K and Hosono H 2010 Josephson junction in cobalt-doped $BaFe_2As_2$ epitaxial thin films on (La,Sr)(Al,Ta)O_3 bicrystal substrates *Appl. Phys. Lett.* **96** 142507
[40] Zhang X *et al* 2009 Josephson effect between electron-doped and hole-doped iron pnictide single crystals *Appl. Phys. Lett.* **95** 062510
[41] Rotter M, Pangerl M, Vogt M and Johrendt D 2008 Superconductivity and crystal structures of Ba_{1-x} $K_xFe_2As_2$ ($x = 0$–1) *Angew. Chem. Int. Ed.* **47** 7949
[42] Stewart W C 1968 Current–voltage characteristics of Josephson junctions *Appl. Phys. Lett.* **12** 277
[43] McCumber D E 1968 Effect of ac impedance on dc voltage-current characteristics of superconductor weak link junctions *J. Appl. Phys.* **39** 3113
[44] Weihnacht M 1969 Influence of film thickness on d.c. Josephson current *Phys. Stat. Sol.* **32** K169
[45] Lin S Z 2012 Josephson effect between a two-band superconductor with s_{++} or $s_{\pm}$ pairing symmetry and a conventional s-wave superconductor *Phys. Rev.* B **86** 014510
[46] Scheller T *et al* 2012 SNS junctions for ac Josephson voltage standards *Phys. Proc.* **36** 48